

Oxygen transfer from flowing water to microbes in an organic sediment bed

Makoto Higashino · Ben L. O'Connor · Miki Hondzo · Heinz G. Stefan

Received: 2 November 2007 / Revised: 5 June 2008 / Accepted: 16 June 2008 / Published online: 21 August 2008
© Springer Science+Business Media B.V. 2008

Abstract Mass transfer of dissolved oxygen (DO) across a sediment–water interface was investigated using laboratory experiments and a numerical simulation model. DO concentration profiles and velocity profiles were measured with high resolution in a recirculating flume with water flowing at cross-sectional average velocities from 3.5 to 11.5 cm/s over a flat and hydrodynamically smooth organic sediment bed. Parameters extracted from the measurements included (1) the DO penetration depth, (2) the effective diffusion coefficient in the sediment layer, (3) the thickness of the turbulent diffusive boundary layer, and (4) the diffusion coefficients in the diffusive boundary layer. DO penetration depths were less than 1 mm, and diffusive boundary layer thicknesses were less than 8 mm. Diffusion in the sediment porewater system was shown to be essentially molecular. The laboratory data were compared

to results from a deterministic simulation model. The model included explicit descriptions of (1) mass transfer through the diffusive boundary layer above the sediment/water interface, (2) the boundary layer development over the sediment bed of finite length, (3) diffusive transfer in the sediment porewater system, and (4) microbial uptake of DO in the sediment. The model included both water-side and sediment-side mass transport limitations. The control of DO flux could alternate between water-side and sediment-side without discontinuity. Monod-type kinetics was adopted for DO uptake in the sediment. Organic substrate availability in the sediment did not vary over the course of an experiment. A kinetic limitation for organic matter (substrate) was not considered, and microbial activity in the sediment was parameterized by biomass density. Measured and simulated DO concentration profiles showed satisfactory agreement, with some discrepancies at the interface caused by roughness and porosity effects of the sediment surface.

Handling editor: D. Hamilton

M. Higashino
Oita National College of Technology, 1666 Maki,
Oita 870-0152, Japan

Present Address:

B. L. O'Connor
U.S. Geological Survey, Reston, VA, USA

B. L. O'Connor · M. Hondzo · H. G. Stefan (✉)
St. Anthony Falls Laboratory, University of Minnesota,
Minneapolis, MN 55414, USA
e-mail: stefa001@umn.edu

Keywords Benthic processes · Dissolved oxygen · Lake bed · Microbes · Microbial processes · Sediment · Stream bed · Water quality

Notations

C DO concentration
 C_w DO concentration at sediment–water interface
 C_∞ DO concentration in bulk flow
 \bar{C} Time-averaged DO concentration

d	Particle grain size
D	Diffusion coefficient
D_s	Diffusion coefficient in sediment
D_t	Turbulent diffusion coefficient
D_t^+	Normalized turbulent diffusion coefficient
H	Flume half-depth
k_d	First-order decay coefficient
k_{O_2}	Half-saturation coefficient
n	Numerical constant, Eq. 4a
R	Hydraulic radius
Re	Reynolds number
Re_d	Shear Reynolds number
Re_x	Boundary layer Reynolds number
SOD	Sediment oxygen demand
t	Time
u, v	Horizontal and vertical velocity components
u', v'	Fluctuating horizontal and vertical velocity components
\bar{u}, \bar{v}	Time-averaged horizontal and vertical velocity components
u_*	Shear velocity
U_∞	Time-averaged free-stream velocity
U^+	Normalized horizontal velocity
x, y, z	Horizontal, vertical, and transverse coordinates
X	Microbial biomass
X_0	Initial microbial biomass
X_{\max}	Maximum microbial biomass
y^+	Normalized vertical coordinate
Y_c	Effective yield
δ	DO penetration depth
δ_D	Diffusive boundary layer thickness
$\varepsilon^{+,-}$	Scale to indicate above and below sediment–water interface
κ	von Kármán constant
μ	Maximum specific growth rate
ν	Kinematic viscosity
ν_t	Turbulent viscosity
ν_t^+	Normalized turbulent viscosity
ρ	Water density
τ_0	Bed shear stress

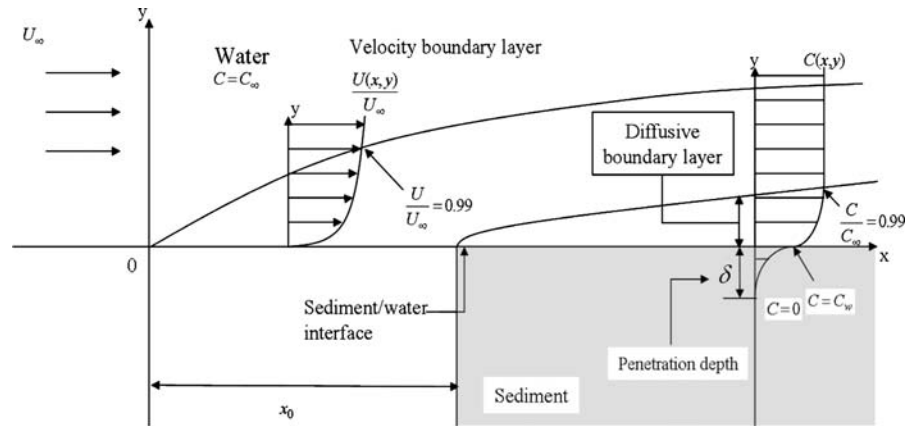
Introduction

Dissolved oxygen (DO) transfer from a water column to the underlying (organic) sediment can affect the DO balance in a stream, lake, or estuary. Oxygen transfer

is mediated by microbial and chemical processes in the sediment, and physical transport processes, i.e., turbulence in the water above the sediment and effective diffusion inside the sediment. Solute transport in the sediment pore system is often treated as molecular, but flow through the sediment pore system can be induced by bedforms, surface waves or turbulent eddies (Boudreau & Jørgensen, 2001). This flow can enhance the oxygen transport in the pore system significantly. Mass transfer from the overlying flowing water to the surface of a flat sediment bed has been studied using the concept of the diffusive boundary layer (Fig. 1) (Rahm & Svensson, 1989; Dade, 1993; Nakamura & Stefan, 1994). The existence and significance of the diffusive boundary layer above the sediment–water interface has been demonstrated in numerous experimental studies (Belanger, 1981; Jørgensen & Revsbech, 1985; Whittemore, 1986; Jørgensen & DesMarais, 1990; Mackenthun & Stefan, 1998; Josiam & Stefan, 1999; Steinberger & Hondzo, 1999; Røy et al. 2002; House, 2003). Many of these studies consider a fully developed diffusive boundary layer, i.e., the DO concentration profile varies only in the vertical direction and not in the direction of the bulk flow. However, experimental and natural aquatic sediment beds have a finite length, and DO concentrations in the overlying water might vary in stream-wise direction.

The overall objective of this study was to collect detailed experimental DO concentration profiles in and above a sediment bed of finite length under different fluid-flow and corresponding shear velocities, and to compare these measurements to simulated DO profiles. The goals were (a) to examine how the near-bed DO profiles respond to changes in flow conditions, and (b) to examine if a detailed boundary layer mass transfer model can simulate the observed DO distributions. A microsensor was used for the DO measurements and a 2-D unsteady mass transport model with microbial kinetics for the simulations. Data were collected for a flat and hydraulically smooth bed, without hyporheic exchange in response to sediment surface topography or water surface waves. The model by Higashino & Stefan (2005a, b) simulates how the DO concentration profiles and the oxygen uptake rates change as a diffusive boundary layer develops. This model incorporates the effect of turbulence above the sediment–water interface and describes the DO uptake rate as a function of the

Fig. 1 Velocity profile $U(x,y)$ and DO concentration profile $C(x,y)$ above a sediment bed of finite length (schematic). Boundary layer growth is also shown



sediment microbial activity. The chemical oxidation of reduced metabolites such as Fe^{2+} , H_2S , or NH_4^+ , is not included in the model.

Experimental methods

Laboratory flume and instrumentation

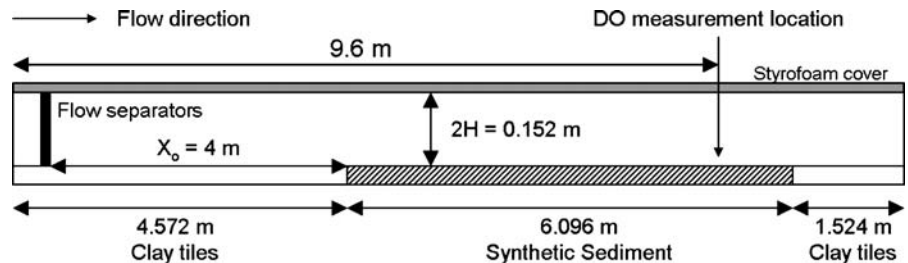
A recirculating flume, 12.19 m long and 0.152 m wide (Fig. 2) was used for the laboratory experiments. The measurement section was located 9.6 m from the inlet, far enough downstream to ensure that the flow field was fully developed (Brodkey & Hershey, 1988). In order to eliminate reaeration at the water surface, styrofoam sections were suspended from the top of the channel creating a water layer with a depth = 0.152 m. Synthetic sediments consisting of sand (81% of dry weight), clay (15%), peat moss (2% sieved to <1 mm), compost (1.95%, sieved to <1 mm), humic acid (0.01%), and dolomite (0.04%) were made according to the procedures described by Walsh et al. (1992) to mimic natural sediments. The synthetic sediment mixture had an organic material content of ~10%. Sediments were mixed dry, wetted, and placed in the channel to a

depth of 0.025 m. The sediment bed was leveled by a scraper attached to a trolley on top of the flume, creating an approximate roughness height of 0.1 mm along the sediment surface. Velocity profiles and DO profiles were measured at the center of the flume at a distance of 0.076 m from either wall.

An acoustic-Doppler velocimeter (ADV, Sontek YSI Inc., San Diego, CA) system was used to measure instantaneous fluid-flow velocities and turbulence characteristics, and a Hydrolab Datasonde 4a (Hach Co., Loveland, CO) water quality probe was used to measure bulk DO concentrations and temperature. The ADV probe measured the x-, y-, and z-velocity components at a frequency of 20 Hz. The velocity data were processed using WinADV software (U.S. Bureau of Reclamation) with filter settings requiring a signal–strength correlation parameter > 70, signal-to-noise ratio > 15; and the phase-space threshold despiking algorithm (Goring & Nikora, 2002).

The micro-scale DO concentration profiles across the sediment–water interface were measured using an OX-10 oxygen microsensor (Unisense, Aarhus, Denmark) attached to a Velmex BiSlide® (Velmex Inc., Bloomfield, NY) positioning system. The location of the sediment–water interface was identified visually with a magnifying glass and then refined using the

Fig. 2 Diagram of experimental flume



observed discontinuity in slope of the measured DO concentration profiles, which is caused by the change in DO diffusion coefficient between the water (D) and the sediments (D_s) as described by Røy et al. (2004). The OX-10 DO microsensor was connected to a Unisense (Aarhus, Denmark) PA2000 picoammeter for signal amplification. DO concentrations were sampled at 10 Hz for a duration of 2 to 5 min. A Butterworth low-pass filter, with a cutoff frequency of 1 Hz, was used to eliminate electronic noise and response-time aliasing.

Experimental flow conditions

Experiments were conducted at cross-sectionally averaged fluid-flow velocities from 3.5 to 11.5 cm/s (Table 1). The Reynolds number (Re) defined by Eq. 1 ranged from 1,330 to 4,380 (Table 1).

$$Re = \frac{U_\infty R}{\nu} \quad (1)$$

where U_∞ is the time-averaged free-stream velocity measured at the half-depth $H = 7.5$ cm above the sediment–water interface, $R = 3.8$ cm is the hydraulic radius and ν is the kinematic viscosity of the water.

The developing boundary layer Reynolds number (Re_x), based on the distance (x) from the inlet ($x = 0$) to the measurement section ($x = 9.6$ m), is defined by Eq. 2. Substituting $x = 9.6$ m and $U_\infty = 3.5$ cm/s into Eq. 2, the Reynolds number for Experiment 1 was $Re_x = 315,000$. Experiments 2 to 5 had Reynolds numbers ranging from $Re_x = 495,000$ to $Re_x = 1,035,000$ (Table 1).

$$Re_x = \frac{U_\infty x}{\nu} \quad (2)$$

On a flat surface the boundary layer flow is expected to change from laminar to turbulent when Re_x exceeds a value on the order of 350,000 to 500,000

(Schlichting, 1979). The Re_x -value for all experiments, except Experiment 1 ($U_\infty = 3.5$ cm/s) was above the turbulent threshold value. It was, therefore, concluded that Experiment 1 was in the transition from laminar to turbulent flow, while Experiments 2 to 5 had fully developed turbulent conditions at the measurement section.

The shear Reynolds number ($Re_d = u_* d/\nu$, where $u_* = \sqrt{\tau_o/\rho}$ is the shear velocity, τ_o is the bed shear stress, ρ is the density of water, and d is the particle grain size) was used to determine whether the sediment bed surface was hydraulically smooth or rough. Based on a measured particle size $d = 0.5$ mm, Re_d values ranged from 0.9 to 2.6. Since the transition from a smooth to a fully rough surface occurs in the range of Re_d values from about 5 to about 70, roughness effects based on particle size were not expected in the laboratory experiments.

Simulation model development

Model of the developing diffusive boundary layer

Fluid-flow above the sediment surface of natural water systems can be induced by gravity (streams and rivers), wind blowing over a water surface (lakes), inflows, withdrawals, or buoyancy (lakes and reservoirs). The fluid motion can be laminar or turbulent. A model to simulate the development of DO concentration profiles near the sediment–water interface of a sediment bed of finite length over which water is flowing, was previously formulated (Higashino and Stefan 2005a, b) and can be summarized as follows.

The DO mass balance in a water column above a sediment bed and beginning at the leading edge of the sediment bed ($x \geq 0$) can be written in the form

$$\frac{\partial \bar{C}}{\partial t} + \bar{u} \frac{\partial \bar{C}}{\partial x} + \bar{v} \frac{\partial \bar{C}}{\partial y} = \frac{\partial}{\partial y} \left[(D + D_t) \frac{\partial \bar{C}}{\partial y} \right] \quad (3)$$

where \bar{C} is the time-averaged DO concentration in the water, \bar{u} and \bar{v} are time-averaged fluid-flow velocities in the longitudinal (x -) and vertical (y -) directions, respectively, D is the molecular diffusion coefficient for DO in water, and D_t is the turbulent diffusivity for DO in water. Longitudinal diffusion and vertical time-averaged advection are considered minor and are ignored. For turbulent flow, a turbulent diffusive boundary layer begins to develop from the leading

Table 1 Experimental flow conditions

Exp. #	U_∞ (cm/s)	u_* (cm/s)	Re	Re_x
1	3.5	0.195	1,330	315,000
2	5.5	0.290	2,100	495,000
3	7.5	0.382	2,860	675,000
4	9.5	0.421	3,620	855,000
5	11.5	0.558	4,380	1,035,000

edge of the reactive sediment ($x = 0$) in the flow direction.

Invoking the Reynolds analogy, D_t is equal to the turbulent diffusivity for momentum or eddy viscosity (ν_t), i.e., $D_t = \nu_t$. Dade (1993) proposed an explicit formulation for eddy viscosity

$$\nu_t^+ = (ny^+)^3 \quad \text{for } y^+ \leq 10 \quad (4a)$$

$$\nu_t^+ = \frac{\kappa y^+ - 2 + \sqrt{(\kappa y^+ - 2)^2 - 4}}{2} \quad \text{for } y^+ > 10 \quad (4b)$$

where n (≈ 0.1) is a numerical constant and κ (≈ 0.4) is the von Kármán constant. Both the eddy viscosity (ν_t) and the vertical coordinate (y) in Eq. 4 were normalized using u_* and ν . The normalized values are

$$\nu_t^+ = \frac{\nu_t}{\nu}, \quad y^+ = \frac{u_* y}{\nu} \quad (5)$$

The profile of the normalized horizontal velocity ($U^+ = u/u_*$) in the water above the sediment–water interface is a function of the normalized eddy viscosity (ν_t^+) and of the normalized vertical coordinate (y^+), and is obtained by Newton's shear law.

$$U^+ = \int_0^{y^+} \frac{dy^+}{1 + \nu_t^+} \quad (6)$$

The diffusive boundary layer thickness increases with distance (x) from the leading edge of the sediment bed, and the rate of growth diminishes with distance. If the depth of the flowing water is finite (total depth, $2H = 0.152$ m in the experimental flume), the diffusive boundary layer reaches a more or less constant value (independent of x) at a point far downstream from the edge. At this point the flow field is said to be “fully developed”.

Model of microbial oxygen uptake in the sediment layer

Oxygen uptake inside the sediment depends upon the utilization of oxygen by bacteria decomposing organic matter and oxidation of reduced metabolites, e.g., Fe^{2+} , H_2S and NH_4^+ . In this model, only the microbial oxygen uptake is considered. Oxygen uptake is driven by organic matter decay which is dependent upon either DO concentration or on the organic substrate concentration or on both. Inside the

sediments, the numerical model uses a mass balance of DO, which can be written as

$$\frac{\partial C}{\partial t} = D_s \frac{\partial^2 C}{\partial y^2} - \frac{1}{Y_c} \mu \frac{C}{K_{O_2} + C} X \quad (7)$$

where D_s is the effective vertical diffusion coefficient in the sediments, X is the biomass (concentration) of the aerobic heterotrophs, K_{O_2} is the half-saturation coefficient for DO utilization by microbes, μ is the maximum specific growth rate (DO utilization rate), and Y_c is the effective yield for the microbial utilization of DO.

Monod-type kinetics is adopted for DO uptake (Eq. 7). Since the half-saturation coefficient in Eq. 7 was relatively small compared to the DO in the sediment porewater, the DO dependence became largely zero-order, except when DO was very low. The limitation of microbial DO uptake in the sediment by the availability of organic substrate could be expressed by adding (as a multiplier) a Monod expression for organic matter, similar to that for DO, to the last term of Eq. 7. This is unnecessary, however, because organic substrate availability is not likely to vary with depth in the sediment layer over the short duration of an experiment. Since available organic substrate concentration is essentially constant over a few hours or days, it is included implicitly in the microbial biomass variable X . The model was calibrated for the maximum possible biomass X_{\max} , and a kinetic limitation for organic matter (substrate) was not expressed explicitly, although Westrich & Berner (1984) among others demonstrated the limitation of sulfate reducing bacteria by organic matter availability.

Our approach is different from that of geochemists who study long time periods (years to millennia), while we consider experiments of a few hours or days duration. Geochemists have to assume that microbial populations can be starved and can replicate rapidly. The long-term temporal variability of organic matter availability to the micro-organisms is then important, and the balance of organic matter inside the sediment needs to be tracked by a second, separate mass balance equation in the model. For our experiments it is safe to assume that organic matter is available at a constant and high rate.

Net growth of the aerobic microorganisms inside the sediment can be described by a logistic model, Eq. 8,

$$\frac{dX}{dt} = \left(\mu \frac{C}{K_{O_2} + C} - k_d \right) \left(1 - \frac{X}{X_{\max}} \right) X \quad (8)$$

in which k_d is the first-order decay coefficient. The steady-state solution to Eq. 8 is $X = X_{\max}$. The DO uptake rate given by Eq. 7 will, therefore, be first order with respect to X_{\max} . The value of X_{\max} is related to substrate availability, i.e., the rate at which nutrients become available to the micro-organisms. Organic substrate limitation is implicit in the maximum biomass term (X_{\max}) in Eqs. 7 and 8. The value of X_{\max} was determined by calibration of a simulated to experimental DO concentration profile. A methodology to relate X_{\max} to direct measurements of organic material inside the sediment is still needed.

The input coefficients used in the microbial kinetic model are listed in Table 2. The model used a water temperature of 25°C throughout the water column above the sediment surface and inside the sediment.

Equation 7 also contains a diffusion term. The effective diffusion coefficient for DO in the sediment (D_s) in Eq. 7 is related to the sediment characteristics and to turbulence above the sediment–water interface. Turbulence penetration into the sediment pore system was not considered, and D_s was taken to be constant and equal to 50% of its pure water value, i.e., $D_s = 0.5D$. This value was chosen because only the pore space fraction is available to diffusion (Bear, 1972), and molecules must travel a longer path around the sediment grains (Boudreau & Jørgensen, 2001). Several empirical relationships between D_s and porosity have been proposed (e.g., Boudreau, 1997; Iversen & Jørgensen, 1993). The factor by which D has to be reduced from its value in water is typically from 0.3 to 0.7—based on typical sediment porosities. We have chosen 0.5 because it has been used in other investigations. An experimental validation is provided below.

Table 2 Biokinetic model input parameters

Coefficient	Range and reference	Selected value
K_{O_2} (mg/l)	0.2 a	0.2
μ (d^{-1})	0.72–13.2 b,e	2.4
Y_c (mg X/mg DO)	0.83–1.17 c,d,e	1.0
k_d (d^{-1})	0.1 e	0.1

Coefficient values were taken from the literature: a—Bailey and Ollis (1986), b—Brezonik (1994), c—Eckenfelder (1966), d—McCarty (1975), and e—Rittmann and McCarty (2001)

Numerical solution

A flow velocity field above the sediment–water interface was obtained for laminar flow and for turbulent flow. With this information, the DO mass balance described by Eq. 3 was solved numerically to obtain the DO concentration profiles. In order to simulate the time variation of microbial biomass inside the sediment, Eq. 8 was integrated by the Runge–Kutta method after the DO concentration profile was obtained in each time step. Numerical computations were continued until a quasi-steady state was reached, and only the steady-state results are reported.

Initial conditions for the numerical simulations were established as follows: (a) the initial DO concentration was taken to be the free-stream DO concentration (C_∞), i.e., $C = C_\infty$, everywhere in the water, and zero, i.e., $C = 0$, everywhere inside the sediment; (b) the initial microbial biomass was assumed to have a value X_0 everywhere inside the sediment. The boundary condition in the water was $C = C_\infty$ at $y = \delta_D$, where δ_D is the thickness of the diffusive boundary layer. The DO concentration inside the sediment was set as $C = 0$ at $y = -20$ mm based on the experimental results by House (2003).

The DO concentration at the sediment–water interface (C_w) for each grid in the streamwise direction and in each time step was required for the DO mass balance equations in the water column and inside the sediment, and was calculated by considering the continuity of the DO flux at the sediment–water interface. In order to obtain a steady-state microbial biomass profile inside the sediment, the computer program was run until biomass levels did not change significantly.

Results

Model calibration for maximum biomass (X_{\max})

The maximum possible biomass concentration inside the sediment (X_{\max}) was not measured (there is currently no known methodology). It was determined by calibration of simulated to experimental DO concentration profiles. Data from one of the five experiments were chosen for this purpose. Experiment 2 was used because its mean flow velocity is about half of the highest velocity tested (Table 1). Figure 3

gives simulated DO concentration profiles for $u_* = 0.29$ cm/s (Experiment 2) at different X_{\max} values (100, 200, 1,000, 1,200, and 1,500 mg/l), and experimental data. For the smallest X_{\max} values (100 and 200 mg/l), the simulated DO profiles penetrate much deeper into the sediment than shown by the measurements. When X_{\max} is large (1,000, 1,200 and 1,500 mg/l), simulated DO concentration profiles agree well with experimental results; they also become practically independent of X_{\max} indicating that DO levels in the sediment are diffusion limited; based on the root mean square error $RMSE = 0.052$ and the regression coefficient $r = 0.99$ between measurements and simulations, X_{\max} was taken to be on the order of 1,000 mg/l for all model simulations. RMSE-values for several X_{\max} -values are given in Table 3. RMSE is dimensionless because it is based on the normalized DO concentrations C/C_{∞} .

Measured velocity profiles $u(y)$ and estimated shear velocities (u_*)

The shear velocity (u_*) in each experiment was estimated by applying the log-law to the measured

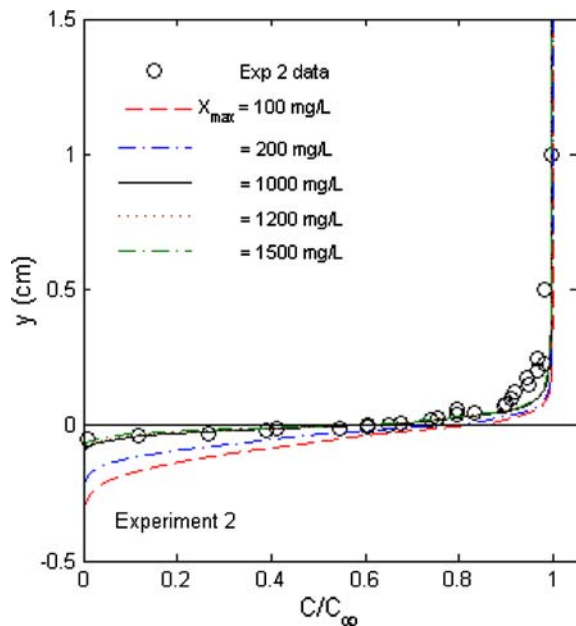


Fig. 3 Experimental DO concentration profile $C(y)$ for Experiment 2 ($u_* = 0.290$ cm/s) and associated simulated DO profiles for maximum biomass concentrations, $X_{\max} = 100$ –1,500 mg/l. Distance y is measured from the sediment surface. Concentration is normalized to the concentration in the overlying water

Table 3 Root mean square error (RMSE) between measured and simulated normalized DO profiles for Experiment 2 near the sediment/water interface for maximum microbial biomass X_{\max} from 100 to 1,500 mg/l

X_{\max} (mg/l)	100	200	1000	1200	1500
RMSE (-)	0.20	0.15	0.051	0.054	0.061

time-averaged velocity profiles in the flowing water. When these velocities were normalized by u_* and v (wall-scaling) for each experiment, the data within the log-law region of the flow ($y^+ > 50$) collapsed more or less onto one line (Fig. 4) indicating that the estimate of u_* for each experiment was appropriate. Below the logarithmic region of the flow, the scaled-velocity profiles diverged, especially for Experiment 1 with the lowest fluid-flow velocities. Turbulence intermittency near the sediment–water interface is the suspected cause.

Estimating the turbulent diffusion coefficient in the diffusive boundary layer

Eddy viscosity (ν_t) was estimated from the slope of the time-averaged velocity profile and the fluctuating u and v velocity components, u' and v' , respectively.

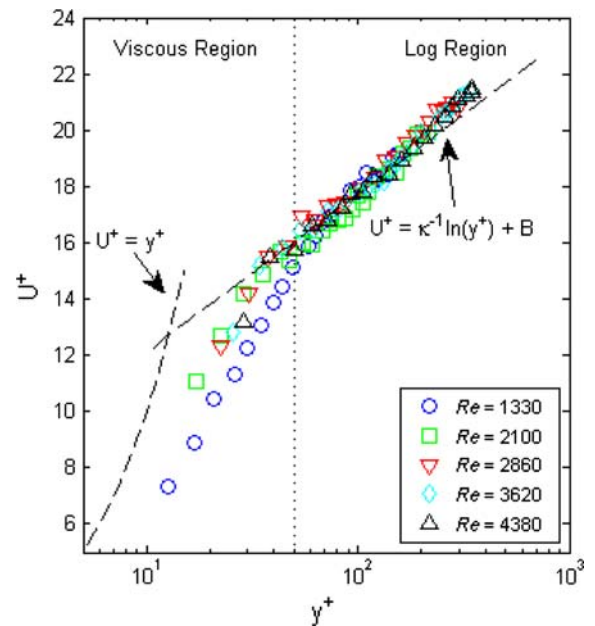


Fig. 4 Log-law velocity profile for ADV data. U^+ is normalized velocity in the water and y^+ is normalized distance from the sediment surface

$$v_t = \frac{\overline{u'v'}}{\left(\frac{\partial \bar{u}}{\partial y}\right)} \quad (9)$$

ADV measurements of the fluctuating u and v velocity components were not possible close to the sediment surface. Therefore, v_t was also estimated using the measured DO profiles. In order to do this, the slopes of the DO profiles $C(y)$ at the sediment–water interface ($y = 0$) and at a distance (y) above the sediment–water interface were calculated. The ratio of the two slopes is equal to v/v_t because the vertical DO flux in the diffusive boundary layer above the sediment surface is constant if no significant DO sink exists in the diffusive boundary layer. With $D_t = v_t$ one obtains

$$v_t = \frac{\left(\frac{\partial \bar{C}}{\partial y}\right)_{y=0}}{\left(\frac{\partial \bar{C}}{\partial y}\right)_{y=y}} D \quad (10)$$

The eddy viscosity (v_t^+), and hence the turbulent diffusion coefficient $D_t^+ \approx v_t^+$ on the water-side, was also modeled as a function of distance from the sediment–water interface y using the equations given by Higashino & Stefan (2005a). Experimental values of v_t computed from the velocity data (Eq. 9) and of D_t computed from the DO data (Eq. 10) can be compared with the model result for v_t in Fig. 5.

DO concentration profiles $C(y)$ near the sediment–water interface

DO concentration profiles on either side of the sediment–water interface were modeled under the fluid-flow conditions given in Table 1. For Experiments 3 through 5 ($u_* = 0.38, 0.47,$ and 0.56 cm/s, respectively), measured DO concentration profiles matched modeled results (Fig. 6 and Table 4).

The measured and simulated DO concentration profiles for Experiment 1 ($u_* = 0.195$ cm/s) are shown in Fig. 7. As the flow over the sediment–water interface was in the transition from laminar to turbulent flow in Experiment 1, two simulated DO concentration profiles (one for laminar flow and one for fully turbulent flow) are shown for comparison. The experimental data fall between the two simulated lines of laminar and turbulent flow. Neither the laminar nor the turbulent flow model is appropriate for this experimental condition. The mean residuals between the measurements and the two models

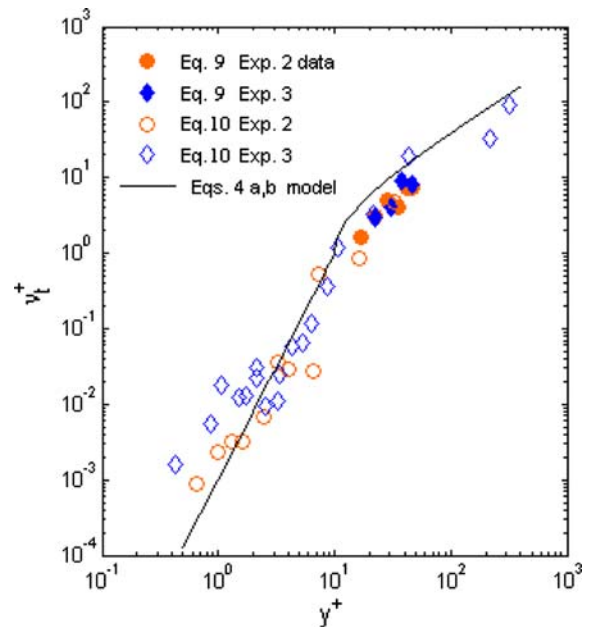


Fig. 5 Experimental and modeled eddy viscosity or diffusivity profile. v_t^+ is normalized eddy viscosity or diffusivity in the water and y^+ is normalized distance from the sediment surface

have opposite signs for the laminar and the turbulent flow model, respectively, and the RMSE values are quite large (Table 5). The simulated diffusive boundary layer thickness for the laminar flow (7 mm) is much thicker than that for the turbulent flow (~ 2 mm); the experimental data show a diffusive boundary layer thickness of ~ 7 mm, which matches the laminar flow condition (Fig. 7). The DO concentration profile on the sediment-side is much better matched by the turbulent flow model including the DO concentration at the sediment–water interface (C_w/C_∞) which is about $C_w/C_\infty = 0.4$ for the turbulent flow, but only $C_w/C_\infty = 0.1$ for the laminar flow. The experimental DO concentration data confirm that the flow above the sediment–water interface in Experiment 1 is in the transition region between laminar and turbulent flow and that the DO mass transfer is controlled by turbulence intermittency, for which mass and momentum transfer models are not well developed.

Diffusive boundary layer thickness (δ_D)

The diffusive boundary layer is located on the water-side above the sediment surface (Fig. 1). Its thickness (δ_D) diminishes significantly as the shear velocity increases as can be seen in Figs. 3, 6, and 7. The diffusive boundary

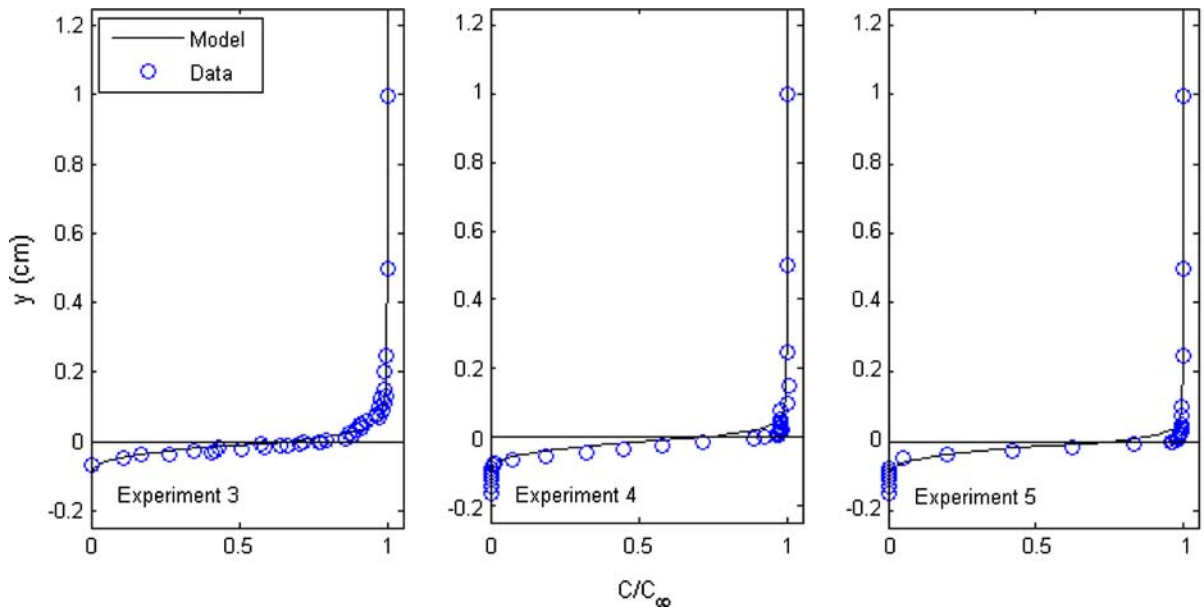


Fig. 6 Experimental and simulated DO concentration profiles. Distance y is measured from the sediment surface. Experiment 3 (left): $u_* = 0.382$ cm/s, Experiment 4 (center): $u_* = 0.471$ cm/s, Experiment 5 (right): $u_* = 0.558$ cm/s

Table 4 Summary statistics between measured and simulated normalized DO concentration profiles for Experiments # 3, 4 and 5

Experiment number	RMSE (–)	r	MR (–)
3	0.0410	0.99	0.0156
4	0.0883	0.99	0.0532
5	0.0810	0.99	0.0449

RMSE, Root mean square error; r , Regression coefficient; MR, Mean residual between measurements and simulations

layer thickness (δ_D) is difficult to measure because of the very gradual transition of the concentration profile to its free-stream value C_∞ . One option is to define δ_D as the distance from the sediment–water interface to the point where the DO concentration is $C(\delta_D)/C_\infty = 0.99$ or 0.98. The choice is important, because if 0.99 is replaced by 0.98 the diffusive boundary layer thickness for Experiment 2 is reduced from 7.5 to 2.3 mm and fits the simulated value much better.

The simulated diffusive boundary layer in the water above the sediment–water interface is much thicker for the laminar flow than for the turbulent flow (7 mm vs. ~ 2 mm in Fig. 7). Experimental and simulated diffusive boundary layer thicknesses (δ_D) for the turbulent flow in Experiments 2 to 5 are plotted against u_* in Fig. 8. Trends are similar, but the extent of the agreement varies with the definition

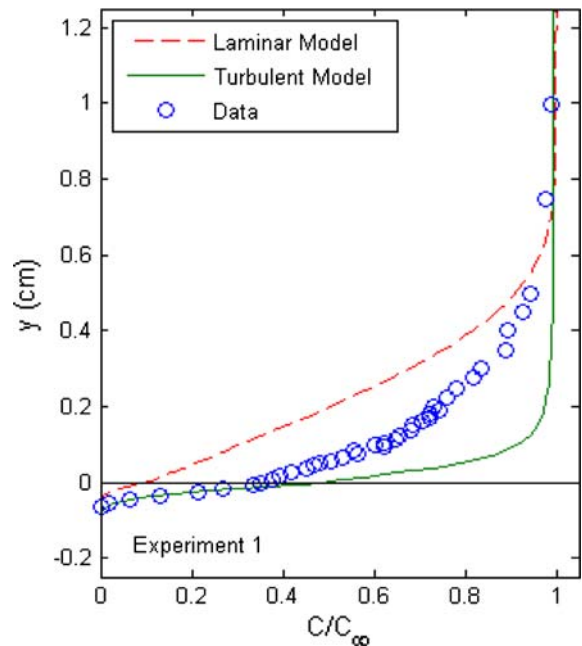


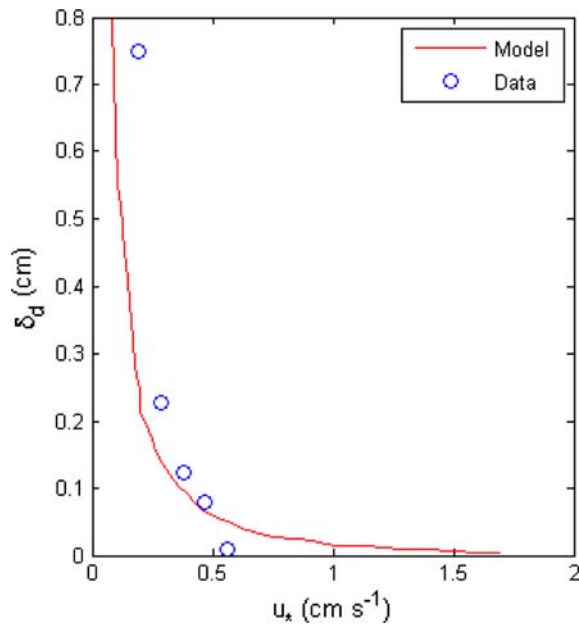
Fig. 7 Experimental and associated simulated DO concentration profiles for Experiment 1 ($u_* = 0.195$ cm/s). Simulated DO concentration profiles are shown for a laminar and a turbulent boundary layer. Distance y is measured from the sediment surface

of (δ_D) and the accuracy of the DO measurements (a DO measurement that is accurate to within 1% is difficult to achieve).

Table 5 Summary statistics between measured and simulated normalized DO concentration profiles for Experiment #1

	RMSE (–)	<i>r</i>	MR (–)
Laminar flow model	0.233	0.94	0.209
Turbulent flow model	0.191	0.94	–0.158

RMSE, Root mean square error; *r*, Regression coefficient; MR, Mean residual between measurements and simulations

**Fig. 8** Dependence of experimental and simulated diffusive boundary layer thickness (δ_D) on shear velocity

Penetration depth into the sediment layer (δ)

The experimental and simulated penetration depths (δ) of DO in the sediment are less than 1 mm (Figs. 3, 6, and 7). The value of δ depends on its definition, but not as strongly as for the diffusive boundary layer thickness (δ_D). If $C(\delta)/C_\infty = 0.01$ is used, the simulated penetration depth is nearly constant at $\delta = 0.7$ mm, while the observed values vary from $\delta = 0.65$ to 0.76 mm.

Effective diffusion coefficient in the sediment layer (D_s)

In the simulation model, the effective vertical diffusion coefficient of DO in the sediment (D_s in Eq. 7) was taken to be constant and equal to 50% of its pure

water value to account for porosity and tortuosity. The experimental DO profiles were used to verify this assumption. The sediment oxygen demand (SOD) flux is continuous across the sediment–water interface. Above the sediment–water interface SOD can be calculated as

$$\text{SOD} = -D(\partial\bar{C}/\partial y)_{y=+\varepsilon} \quad (11)$$

The slope $(\partial\bar{C}/\partial y)_{y=+\varepsilon}$ is calculated from the DO profile at a very short distance $y = +\varepsilon$ above the sediment–water interface. Below the sediment–water interface SOD is given by

$$\text{SOD} = -D_s(\partial\bar{C}/\partial y)_{y=-\varepsilon} \quad (12)$$

where the slope $(\partial\bar{C}/\partial y)_{y=-\varepsilon}$ is calculated from the DO profile at a very short distance $y = -\varepsilon$ below the sediment–water interface. Using Eqs. 11 and 12 the ratio D_s/D can be calculated from the ratio of the concentration gradients $\partial\bar{C}/\partial y$ above and below the sediment–water interface. These slopes were calculated from the experimental data for Experiments 1–3 over distances of 0.1, 0.2, and 0.3 mm above and below the sediment–water interface. The nine D_s/D values obtained had an average of 0.45 and a range from 0.27 to 0.67. This experimental result confirms that the originally selected value $D_s/D = 0.50$ was a good choice.

DO concentration at the sediment–water interface (C_w)

In Experiment 1 the simulated normalized DO concentration at the sediment–water interface is about $C_w/C_\infty = 0.10$ for the laminar flow and $C_w/C_\infty = 0.40$ for the turbulent flow. As u_* was increased from Experiments 1–5 (Table 1), more intensive turbulent transport in the diffusive boundary layer increased the C_w/C_∞ value. For Experiment 5 with $u_* = 0.558$ cm/s, the DO concentration at the sediment–water interface was $C_w/C_\infty = 0.96$. Measured and simulated C_w/C_∞ values presented in Fig. 9 show some disagreement. The measured value of C_w/C_∞ is very sensitive to measurement errors because of the very strong DO gradient at the sediment water interface (Figs. 3, 6, and 7), and the porous boundary. The experimental sediment was characterized as a hydraulically smooth bed with an approximate roughness height of 0.1 mm. Using the DO concentration gradients at the sediment–water interface

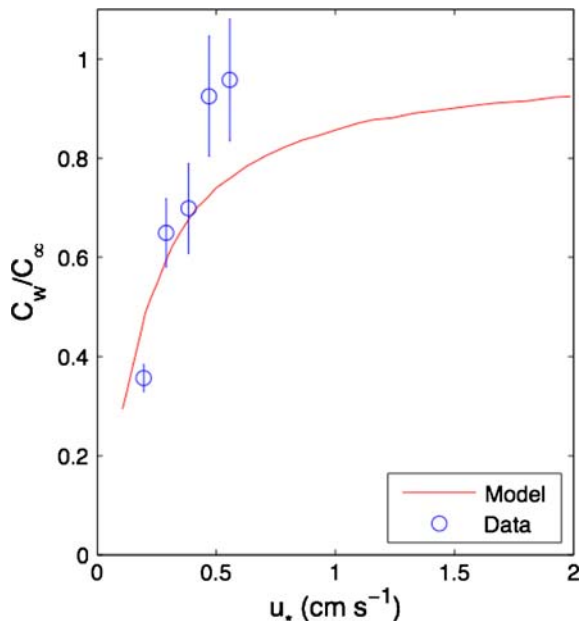


Fig. 9 Dependence of experimental and associated simulated DO Concentrations at the sediment–water interface (C_w/C_∞) on shear velocity (u_*)

and a displacement of 0.1 mm, C_w varies between 7% and 15% of the measured value, which is depicted by the error bars for C_w/C_∞ in Fig. 9.

The combined effects of the bed roughness and the DO concentration gradients are amplified at higher u_* values, where the model tends to under-predict the measurements. This is also a result of the model's treatment of turbulence near the interface. The model expression for eddy viscosity ν_t^+ in Eq. 4a, b under-predicted measured values estimated using Eqs. 9 and 10 for low y^+ values near the interface (Fig. 5). Another significant cause of the discrepancies in Fig. 9 and Fig. 8 is, therefore, most likely the model assumption that there is no turbulence at the sediment–water interface ($y = 0$). Turbulence penetration into the sediment pore system from the flowing water above is ignored.

Discussion

Overall, the agreement between measurements and simulation results is reasonable and acceptable, considering the range of flow velocities considered, resulting in both water- and sediment-side control of the flux. That biomass was a calibration parameter,

undoubtedly contributed to that agreement. Measurements of DO profiles with microprobes, as well as model formulations can account for the discrepancies between observed and simulated DO profiles.

The DO microsensors have a detection limit of 0.01 mg/l and profiles were measured at a resolution of 0.1 mm across the sediment–water interface. Probably the greatest challenge in resolving model results with experimental data is at the sediment–water interface. The model defines a flat boundary that allows for a clear definition of the DO concentration and turbulence at the interface (C_w and ν_t^+ , respectively). While the experiments were conducted on a hydraulically smooth bed, the sediment grains resulted in an uncertainty of the interface of approximately ± 0.1 mm. This uncertainty, in combination with strong vertical DO concentration and ν_t^+ gradients near the sediment–water interface, generated potential errors in quantifying the DO flux. These measurement limitations are not as significant in the calibrated simulation model.

Limitations of the model formulation have been pointed out by Higashino & Stefan (2005a, b). The logistic model for the microbial growth, in particular, may be too restrictive. The model specifications include DO transfer rates across a sediment–water interface which can be limited by water-side or sediment-side transfer. Serious limitations in DO transfer occur when turbulence in one or both of the two adjacent boundary layers becomes suppressed, and molecular transfer becomes dominant. Turbulent diffusivities are specified on the water-side (diffusive boundary layer) and molecular diffusivity is specified on the sediment-side (porewaters) of our model.

Eddy diffusivities in the diffusive boundary layer are formulated based on theories and observations for flat and smooth solid walls (Dade 1993). The “real” sediment–water interface may be neither totally flat nor smooth. Three-dimensional surface patterns may exist on the sediment–water interface, and may have a significant effect (Røy et al. 2002). More importantly, the sediment–water interface is porous and permeable to turbulence. Turbulence penetration across the sediment–water interface into the sediment pore-space is not accounted for in the model. This is believed to be the reason for the discrepancies in Fig. 9. Higher turbulence levels near the sediment–water interface will tend to bring the normalized DO concentrations closer to 1.0 as is shown by the experimental data. In

the model, turbulence is reduced to zero at the sediment–water interface, and that is why the modeled normalized DO concentrations are lagging. In other words a more realistic turbulence model for the uppermost part of the sediment is needed. This model should include turbulence penetration into the sediment pores. The same model improvement would also reduce the discrepancies in Fig. 8 because higher turbulence levels in the diffusive boundary layer would make the diffusive boundary layer thinner. In summary, reducing turbulence at the sediment–water interface ($y = 0$) to zero seems to give an unrealistic model with adverse model results in Figs. 8 and 9. As a next step, the linkage between sediment characteristics (grain size, porosity, tortuosity, etc.) and diffusivities (in the water-side boundary layer and in the uppermost sediment pores) needs to be explored.

Flexibility exists in the model with regard to specification of biomass. Biomass was a calibration parameter, but can be linked to nutrient availability, temperature, as well as sediment characteristics, such as grain size, porosity, etc. It is conceivable that multiple substrate limitations come into play. As turbulence facilitates DO transport into the sediment, availability of DOC or acetate may become an effective control for the growth of microbial biomass. In extreme cases, toxicity may be a limiting factor.

Conclusions

A new DO transport model that incorporates turbulent diffusion from the overlying water into the sediment pores, and microbial uptake of DO in the sediment was presented (Higashino & Stefan (2005a, b)). The model goes beyond the Sherwood number versus Reynolds number relationship for water-side physical transport limited DO transfer (e.g., Steinberger & Hondzo, 1999). It incorporates the oxygen sink on the sediment-side explicitly. The strength of the model is that it does not specify a priori whether the water-side or the sediment-side is limiting the DO transfer process. It can handle a continuous transition from a highly turbulent water flow, where the oxygen uptake on the sediment-side exerts complete control over DO transfer rates, to a very low velocity flow where DO supply from the water-side to the sediment becomes the dominant limitation. The reliability and sensitivity of the model for estimation of oxygen transfer at a

sediment–water interface was investigated by comparing simulated and measured DO concentration profiles under varying fluid-flow conditions. The comparison showed acceptable agreement and consistency between simulated and measured DO concentration profiles. Requirements and avenues for further model refinement have been pointed out.

Acknowledgments The experiments described in this article were supported by the STC program of the National Science Foundation through the National Center for Earth-surface Dynamics (under the agreement Number EAR-0120914). We thank Chris Ellis for technical and software support during the experiments. Dr. B. Boudreau provided helpful comments on an early version of the manuscript. Two anonymous reviewers suggested editorial improvements of the final manuscript. We thank these individuals and organizations for their support.

References

- Bailey, J. E. & D. F. Ollis, 1986. *Biochemical Engineering Fundamentals*, Second ed. McGraw-Hill, New York, NY.
- Bear, J., 1972. *Dynamics of Fluids in Porous Media*. American Elsevier.
- Belanger, T. V., 1981. Benthic oxygen demand in lake Apopka, Florida. *Water Research* 15: 267–274.
- Boudreau, B. P., 1997. A one-dimensional model for bed-boundary layer particle exchange. *Journal of Marine Systems* 11: 279–303.
- Boudreau, B. P. & B. B. Jørgensen, 2001. (eds.). *The Benthic Boundary Layer: Transport Processes and Biogeochemistry*. Oxford University Press, UK, 404 pp.
- Brezonik, P. L. 1994. *Chemical Kinetics and Process Dynamics in Aquatic Systems*. CRC Press, 754 pp.
- Brodkey, R. S. & H. C. Hershey, 1988. *Transport Phenomena*. McGraw-Hill, New York.
- Dade, W. B., 1993. Near-bed turbulence and hydrodynamic control of diffusional mass transfer at the sea floor. *Limnology and Oceanography* 38(1): 52–69.
- Eckenfelder, W. W., 1966. Biological treatment of waste water. *Advances in Hydroscience* 3: 153–190.
- Goring, D. G. & V. I. Nikora, 2002. De-spiking acoustic Doppler velocimeter data. *Journal of Hydraulic Engineering* 128(1): 117–126.
- Higashino, M. & H. G. Stefan, 2005a. Oxygen demand by a sediment bed of finite length. *Journal of Environmental Engineering* 131(3): 350–358.
- Higashino, M. & H. G. Stefan, 2005b. Sedimentary microbial oxygen demand for laminar flow over a sediment bed of finite length. *Water Research* 39: 3153–3166.
- House, W. A., 2003. Factors influencing the extent and development of the oxic zone in river-bed sediment. *Biogeochemistry* 63: 317–333.
- Iversen, N. & B. B. Jørgensen, 1993. Diffusion coefficients of sulfate and methane in marine sediments. *Geochimica et Cosmochimica Acta* 57: 571–578.

- Jørgensen, B. B. & D. J. DesMarais, 1990. Diffusive boundary layer of sediments: Oxygen microgradients over a microbial mat. *Limnology and Oceanography* 35(6): 1343–1355.
- Jørgensen, B. B. & N. P. Revsbech, 1985. Diffusive boundary layers and the oxygen uptake of sediment and detritus. *Limnology and Oceanography* 30(1): 111–122.
- Josiam, R. & H. G. Stefan, 1999. Effect of flow velocity on sediment oxygen demand: comparison of theory and experiments. *Journal of the American Water Resources Association* 35(2): 433–439.
- Mackenthun, A. & H. G. Stefan, 1998. Effect of flow velocity on sediment oxygen demand: experiments. *Journal of Environmental Engineering* 12(3): 222–230.
- McCarty, P. L., 1975. Stoichiometry of biological reaction. *Progress in Water Technology* 7(1): 157–172.
- Nakamura, Y. & H. G. Stefan, 1994. Effect of flow velocity on sediment oxygen demand: theory. *Journal of Environmental Engineering* 120(5): 996–1016.
- Rahm, L. & U. Svensson, 1989. On the mass transfer properties of the benthic boundary layer with an application to oxygen fluxes. *Netherlands Journal of Sea Research* 24(1): 27–35.
- Rittmann, B. E. & P. L. McCarty, 2001. *Environmental Biotechnology: Principles and Applications*. McGraw-Hill Higher Education, Boston, Massachusetts.
- Røy, H., M. Huettel & B. B. Joergensen, 2002. The role of small-scale sediment topography for oxygen flux across the diffusive boundary layer. *Limnology and Oceanography* 47(3): 837–847.
- Røy, H., M. Huettel & B. B. Joergensen, 2004. Transmission of oxygen concentration fluctuations through the diffusive boundary layer overlying aquatic sediments. *Limnology and Oceanography* 49(3): 686–692.
- Schlichting, H. 1979. *Boundary-Layer Theory*. McGraw-Hill.
- Steinberger, N. & M. Hondzo, 1999. Diffusional mass transfer at the sediment–water interface. *Journal of Environmental Engineering* 125(2): 192–200.
- Walsh, G. E., D. E. Weber, L. K. Esry, M. T. Nguyen, J. Noles & T. Albrecht, 1992. Synthetic substrata for propagation and testing of soil and sediment organisms. *Pedobiologia* 36: 1–10.
- Westrich, J. T. & R. A. Berner, 1984. The role of sedimentary organic matter in bacterial sulfate reduction: the G model tested. *Limnology and Oceanography* 29(2): 236–249.
- Whittemore, R., 1986. The significance of interfacial water velocity on the measurement of sediment oxygen demand. In Hatcher, K. (ed.), *Sediment Oxygen Demand. Processes Modeling and Measurement*. Institute of Natural Resources, University of Georgia, Athens, GA: 63–74.